ES Materials and Manufacturing
DOI: https://dx.doi.org/10.30919/esmm5f554

Wavelet Power and Shannon Entropy Applied to Acoustic Emission Signals for Corrosion Detection and Evaluation of Reinforced Concrete

Jinrui Zhang,[1] Ziye Kang,[2] Dongshuai Hou,[3] Biqin Dong[4] and Hongyan Ma[5,*]

Abstract

Acoustic emission (AE) signals detected from corrosion test on a steel reinforced concrete beam subjected to the coupling effects of corrosive wet-dry cycles and static load are analyzed by power spectral density, wavelet transform, and Shannon entropy. The degradation process of the corroded reinforced concrete beam can be divided into four stages on the basis of the accumulated event number (AEN). Due to the difference of material properties, steel reinforcement and concrete matrix have distinguished AE features. The time-frequency characteristics of AE signals can reflect the microstructural degradation mechanism of steel corrosion and concrete cracking. The corrosion evaluation entails investigating the evolution of the wavelet power mathematically by Shannon entropy. The frequency-entropy clearly exhibits the relative power distribution of AE signal in a certain frequency region. With the accumulation of steel corrosion and concrete deterioration, the increment of the overall entropy integration is considerably apparent. The variation of frequency-entropy curve reveals the corrosion revolution of the reinforced concrete members under static load, which is represented by a transforming from corrosion-induced micro cracking to load-induced localized cracking.

Keywords: Corrosion; Reinforced concrete; Acoustic emission; Wavelet power; Shannon entropy.
Received: 20 September 2021; Accepted: 23 October 2021.
Article type: Research article.

1. Introduction

Corrosion of steel reinforcement is one of the primary factors affecting the load-carrying capacity and durability of reinforced concrete structures.[1-3] Steel corrosion not only decreases the effective cross-section area of reinforcement, but also causes stress concentrations inside the steel rebar, resulting in the reduction of ductility and serviceability of reinforced concrete structures.[4-6] Moreover, expansive corrosion products generate tensile stress and cracks in the concrete that protects the reinforcement. Cracks can accelerate the ingress of external erosive substances, such as carbon dioxide, chloride ions and sulfate ions, leading to accelerated steel corrosion or other types of concrete deterioration.[7] Eventually, the highly porous and weak corrosion products tend to lessen the bonding strength between steel rebar and (degraded) concrete matrix, reducing the load-carrying capacity of the structural members and potentially causing unexpected failures of reinforced concrete structures.[8]

Detection and evaluation of steel corrosion, especially early-stage corrosion, in reinforced concrete structures has been attracting worldwide attention. A great deal of research has been done on corrosion evaluations, including half-cell potential, galvanic current, electromagnetic technique, optical fiber sensing, acoustic emission (AE) and so forth.[9-14] Different from other detection techniques that evaluate certain status, AE is designed to investigate dynamic behaviors in materials and structures.[15] It has been reported that identifications of corrosion initiation and concrete cracking by AE are very effective.[16-18] Moreover, AE technique affords an earlier warning than conventional electrochemical methods, and is also ideal for on-line continuous monitoring of dynamic corrosion process in reinforced concrete, especially for the

[1] *State Key Laboratory of Hydraulic Engineering Simulation and Safety, Tianjin University, Tianjin 300072, China.*
[2] *School of Civil Engineering, Tianjin University, Tianjin 300072, China.*
[3] *Department of Civil Engineering, Qingdao Technological University, Qingdao 266033, China.*
[4] *Guangdong Province Key Laboratory of Durability for Marine Civil Engineering, Shenzhen University, Shenzhen 518060, China.*
[5] *Department of Civil, Architectural and Environmental Engineering, Missouri University of Science and Technology, Rolla, MO 65401, United States.*
**Email:* mahon@mst.edu (H. Ma)

hardly accessible parts of a structure.[19]

AE can be stress wave radiations generated by steel corrosion, concrete cracking or interfacial debonding in reinforced concrete structural members.[20] Traditional AE parameters such as accumulated event number (AEN), event rate (ER), rise angle (RA) and average frequency (AF), have been widely accepted as indicators for crack initiation and growth.[21-23] In addition to the basic investigations on evolution and development of traditional signal-based AE parameters, time-frequency analysis of AE signals has drawn widespread concern from researchers.[24-26] The time-frequency information of AE signals has close relationships with the instantaneous evolutions of steel corrosion and concrete cracking, so that wavelet transform (WT) is considered a promising approach for analyzing AE signals induced by damages in reinforced concrete.[27-29] In addition, Shannon entropy is an effective tool to quantitatively describe the energy distribution of wavelet coefficients.[30-32] It thus has a big potential to be used in steel corrosion detection and interpretation, although relevant studies have been scarce. In this study, it is speculated that the combination of wavelet transform and Shannon entropy can generate a powerful tool to extract the features of AE signals (including distinguish the signals induced by steel corrosion from that induced by loading), so as to reveal more detailed characteristics of steel corrosion in reinforced concrete.

This paper presents an investigation on steel corrosion detection and evaluation of loaded reinforced concrete structural members subjected to wet-dry cycles with NaCl solution by AE technique. Cement-based piezoelectric sensors are employed for data collection of AE signals, because of its improved sensitivity and durability in concrete materials. Two signal-processing techniques – wavelet transform and Shannon entropy – are applied and integrated to analyze AE signals coming from corrosion induced damages of reinforced concrete.

2. Experiment and measurement

2.1 Cement-based piezoelectric sensor

The cement-based piezoelectric sensors, featuring the advantage of high sensitivity and good compatibility with concrete matrix, are suitable to be applied for damage detection in concrete materials and structural members.[33-35] In this study, the cement-based piezoelectric sensor was employed for AE detection and the detailed fabrication process of the sensor was presented in Ref.[36] The time and frequency response of the cement-based piezoelectric sensor subjected to a standard Hsu-Nielsen pencil lead break is illustrated in Fig. 1. The pencil lead break is an artificial acoustic source that can generate reproducible acoustic events. In the test, a pencil lead is broken against the specimen under a defined angle, aided by a special show (specified in ASTM E976). The calibration results certify the broadband characteristics of the cement-based piezoelectric sensor from 20 to 500 kHz, which ensures the accuracy of the monitored AE signals generated by steel corrosion and concrete cracking.[37]

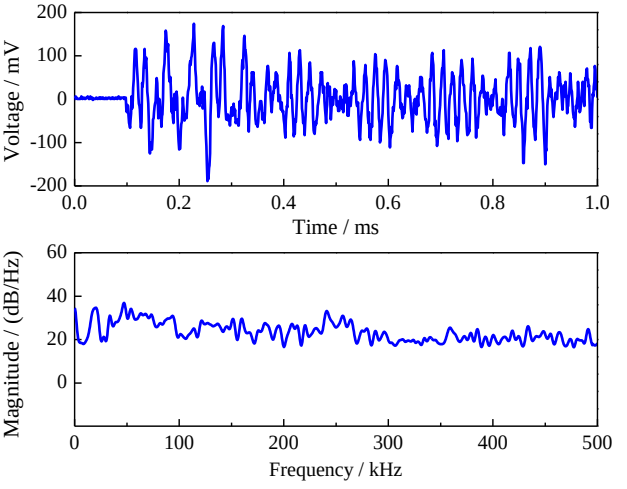

Fig. 1 The time and frequency response of the cement-based piezoelectric sensor.

2.2 Experimental preparation and setup

Two identical reinforced concrete beams were prepared (2000 × 200 × 120 mm) in this experiment, each of which was reinforced by three reinforcing steel bars – two in the compressive zone (12 mm in diameter) and one in the tensile zone (16 mm in diameter) with a concrete cover of 30 mm. The mix proportion of concrete is listed in Table 1, in which cement is an ordinary Portland cement conforming to ASTM C150 Type I, sand is a river-sourced silica sand, and coarse aggregate is crushed granite with a maximum particle size of 9.5 mm. One beam was used to measure the ultimate bearing capacity of the beam, and the result indicated that the ultimate bending moment was 12.8 kN·m. Then, the other one, as shown in Fig. 2, was subjected to the static load of 30% ultimate bending moment coupled with 3% NaCl solution (stored in a pond made with PVC frame and hot-melt glue) in the tension zone to simulate the service status of a reinforced concrete structure in marine environment. In order to accelerate the corrosion process, 3-day wet (soaked in NaCl solution) and 4-day dry (25 ± 1 °C, 50 ± 2% relative humidity) cyclic tests were executed on the reinforced concrete beam. The static bending moment was applied through a four-point bending device sketched in Fig. 2. The support displacement was measured by LVDT to monitor the deflection of the beam in a duration of 16 weeks (or wet-dry cycles).

Table 1. Mix proportions of concrete material / (kg/m^3).

Cement	Water	Superplasticizer	Sand	Aggregate
620	236	0.62	620	930

The cement-based piezoelectric sensors were affixed to the surface of the tensile reinforcement to monitor the AE signals generated by steel corrosion and concrete cracking. In this way, the tensile reinforcement serves as a wave guide to mitigate the negative effects of scattering and reflection of acoustic

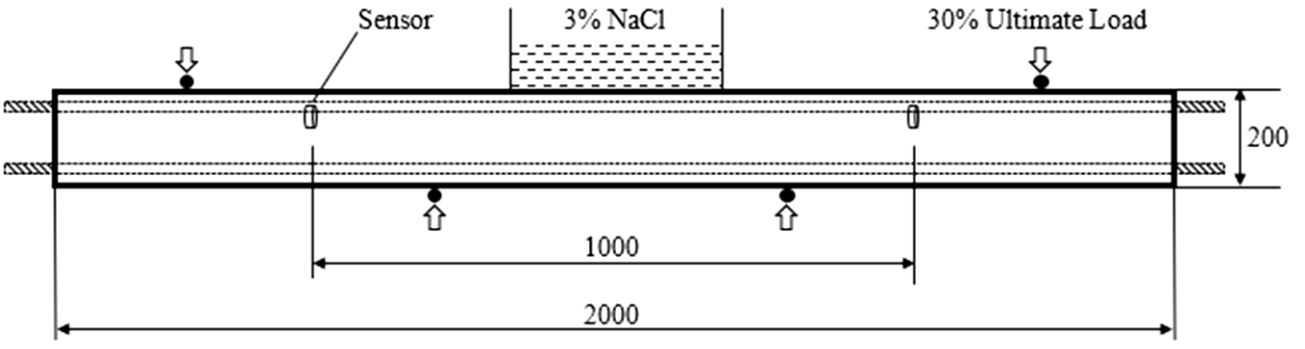

Fig. 2 Measurement apparatus of reinforced concrete beam under accelerated corrosion condition.

signals during their propagation. The trigger threshold of the AE acquisition system was set as 10 mV, just surpass the background noise.[38] The triggered AE signals were modulated by a pre-amplifier (gain of 40 dB, bandwidth of 30 kHz-1 MHz) and then transmitted to the data acquisition system with a sampling frequency of 2 MHz. The accumulated event number, power spectral density, wavelet power and Shannon entropy were employed as the indicators for steel corrosion and damage accumulation in reinforced concrete subjected to the accelerated corrosion test.

2.3 Wavelet power

In order to detect and evaluate the corrosion and degradation process of reinforced concrete, an effective computational approach is necessary to analyze the large AE data. AE is a non-stationary, transient and non-linear process, the power spectrum of which changes with time, where short and long-time phenomena coexist. Therefore, wavelet transform, as a time-frequency analysis tool, becomes one of the most promising techniques in the field of AE signal processing. In this study, continuous wavelet transform (CWT) is applied to analyze the AE signal and the corresponding CWT of a given signal $f(t)$ in time domain is defined as:

$$wt(a,b) = \frac{1}{\sqrt{a}} \int_{-\infty}^{\infty} f(t) \cdot \psi^* \left(\frac{t-b}{a}\right) \cdot dt \quad (1)$$

where $\psi(t)$ is called the mother wavelet, which should be a square integrable and piece-wise continuous function; $*$ denotes the complex conjugate; a is the scale index controlling the stretch of the analysis window, and b indicates the time shifting. The related wavelet power is defined as:

$$wp(a,b) = |wt(a,b)|^2 \quad (2)$$

The wavelet transform gives the localized information of the spectrum of $f(t)$ with a frequency window.[39] The width of the band pass filter in the CWT is inversely proportional to the scale a. Therefore, the wavelet coefficients at higher scales represent the energy of the AE signal at lower frequencies.[40] The pseudo-frequency F_a corresponding to the scale a is implemented by[41]

$$F_a = \frac{F_c}{a \cdot \Delta} \quad (3)$$

where, F_c and Δ denote the center frequency of a wavelet in Hz and the sampling period, respectively.

The selection of an appropriate mother wavelet for signal decomposition and feature extraction is of great significance for defect diagnosis. As one of the most well-known and widely-used mother wavelet, Morlet wavelet enables the measurement of the localization frequency for signals with faster and slower oscillations, which provides a flexible window that narrows at high frequencies and widens at low frequencies. In this study, the Morlet wavelet was employed as the mother wavelet to analyze the detected AE signals generated by steel corrosion and concrete cracking.

In time domain, Morlet wavelet is expressed as a sine wave multiplied by a Gaussian envelope

$$\psi(t) = e^{i\omega_0 t} e^{\frac{-t^2}{(2\delta^2)}} \quad (4)$$

In frequency domain, the dilated version of Morlet wavelet is given by

$$\Psi(\omega) = \delta\sqrt{2\pi} e^{\frac{-(a\omega-\omega_0)^2\delta^2}{2}} \quad (5)$$

where δ and ω_0 are constants; ω_0 denotes the wavelet center frequency.

2.4 Shannon entropy with frequency

Entropy in information theory is a measurement of unpredictability of information content. The energy distribution of wavelet coefficients can be quantitatively described by Shannon entropy based on the previous research.[42-44] Thence, wavelet transform-based Shannon entropy is an effective technique to extract the key information of AE signals. In this study, CWT is performed to decompose the signal into time-frequency domain. Then, a frequency window slides on the wavelet coefficient matrix to get the frequency information of steel corrosion and concrete cracking in reinforced concrete structures. Thereby, Shannon entropy is calculated at the frequency of scale a, as follows:

$$WP_a = \sum_{b=1}^{N} wp(a,b) \quad (6)$$

$$p_{a,b} = wp(a,b)/WP_a \quad (7)$$

$$Entropy(a) = -\sum_{b=1}^{N} p_{a,b} \cdot log_2 p_{a,b} \quad (8)$$

The Shannon entropy of wavelet coefficients is bounded by

$$0 \le Entropy(a) \le log_2 N \quad (9)$$

where $Entropy(a)$ is the wavelet entropy corresponding to the scale a; a is the scale index (frequency interval related with a); b is the time shifting; N is the number of wavelet coefficients in time series.

3. Results and discussion

3.1 Stages of corrosion-induced deterioration

When steel reinforcement in a concrete structural member is corroded, since the corrosion products (*e.g.* ferrous or ferric oxide) occupy a much larger volume than the original metal, the formation of corrosion products exerts outward expansive pressure on the surrounding concrete materials and leads to tensile/shear stress.[45] When chloride ions are present, the rates of steel corrosion and stress buildup could be accelerated. Once the stress level exceeds the tensile limit of the concrete, corrosion-induced micro-cracks initiate and propagate towards the surface of concrete cover.[46] The sudden release of strain energy during this process (*e.g.* due to cracking) generates stress wave (*i.e.* acoustic emission), which can be collected with the help of the piezoelectric sensors.[47] Further, the status of the corroded steel reinforcement and the reinforced concrete structural member can be evaluated according to the detected AE signals.

The accumulated event number (AEN) of AE signals has been widely accepted as an indicator for structural damage accumulation.[48-50] The AEN detected by the piezoelectric sensors during wet-dry cycles is plotted in Fig. 3. The AEN increases with wet-dry cycles of 3% NaCl solution and eventually reaches 990 times at the end of test. Based on the AEN curve over the sixteen cycles, the degradation process of the reinforced concrete beam can be divided into four stages: Stage I is chloride ions ingress and accumulation; Stage II is corrosion initiation and micro-cracks propagation; Stage III is corrosion rate reduction; Stage IV is reinforcement performance degradation and localized macro-crack growth. This four-stage evolution of damage is consistent with previously published research.[51] Following the evolution of AEN, the deflection variations at the end support of the reinforced concrete beam throughout the sixteen wet-dry cycles are illustrated in Fig. 4.

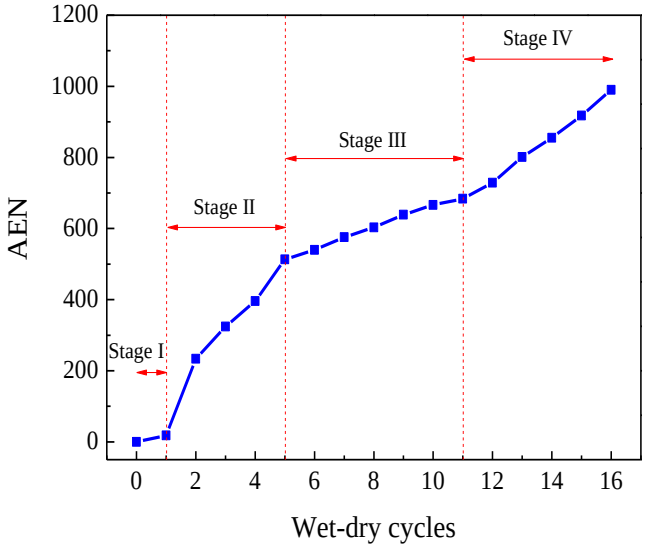

Fig. 3 Accumulated event number (AEN) detected by AE technique during wet-dry cycles.

Normally, 20% of the ultimate bending moment is sufficient to cause cracking in the tension zone of the reinforced concrete members. In this study, the initial cracks induced by the external load (30% of the ultimate bending moment) provide a path for the rapid ingress of corrosive solution into the concrete. However, the increment of AEN is quite slow at the first stage, which means that the steel reinforcement does not corrode immediately even with moisture, oxygen and chloride. This is due to the high alkalinity in the micro pore liquid phase of Portland cement concrete.[52] In such surroundings, a thin passivation layer of insoluble metal oxide/hydroxide can be formed on the surface of steel reinforcement. The dense and impenetrable passive film inhibits the anodic iron dissolution process and reduces the corrosion rate to an unnoticeable level.[53] On the other hand, Fig. 4 shows that the first stage has the largest growth rate of the support displacement, reaching 0.1 mm/cycle. The external load-induced continuous debonding between the tensile reinforcement and concrete matrix causes the stiffness reduction of the reinforced concrete beam, leading to the rapid increase in deformation.[54]

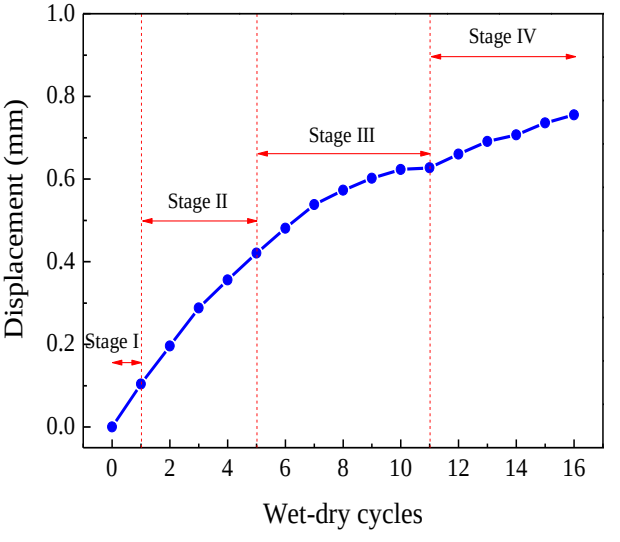

Fig. 4 Support displacement measured by LVDT during wet-dry cycles.

The AEN increases significantly in the second stage and even exceeds 500 times at the end of the fifth wet-dry cycle. The sharp increment of AEN is attributed to the depassivation of the steel surface with the accumulation of chloride ions by wet-dry cycles. The externally invaded NaCl solution can dissolve the stable passive film when $[Cl^-]/[OH^-]$ ratio in the pore solution surrounding the steel surpasses a threshold value, a generally accepted value of which is 0.61.[55] Additionally, the internal stress generated by the external load also accelerates the deterioration of the passive film to some extent. In general, the accelerated corrosion process of the steel reinforcement is a major factor of the sudden and rapid increase of AEN. Correspondingly, the support displacement continuously increases at this stage, resulting from the corrosion-induced structural stiffness reduction.

Nevertheless, the corrosion rate revealed by the growth rate of AEN gradually slows down in the third stage. A reasonable explanation for this phenomenon is that, in this period, the corrosion rate is controlled by the diffusion of oxygen in the corrosion products layer which has become thicker thus prolonged the traveling time of oxygen to the uncorroded steel surface.[56] The corrosion products fill and accumulate in the micro-cracks at the rebar-concrete interface, which can also reduce the rate of oxygen supplementary to the uncorroded surface, resulting in reduction of the corrosion rate of the tensile rebar. It can be clearly seen from Fig. 4 that, similar to the growth trend of AEN, the support displacement measured by LVDT tends to become constant gradually and the variation of support displacement is getting smaller and smaller. In other words, the corrosion status of steel reinforcement at this stage tends to become steady.

Another sudden increase in both AEN and support displacement occurs at the fourth stage, as shown in Figs. 3 and 4. Different from carbonation attack, chlorides act as catalysts causing pitting corrosion on the steel surface.[57] With the accumulation of rust generated over the pit, the loss of the cross-sectional area in pitting corrosion appears rapidly, which critically reduces the load bearing capacity of the reinforced concrete members. The deflection of the concrete beam gradually increases under the external static load, leading to the emergence of new cracks as well as the growth of localized macro-cracks. The fresh cracks generated at this stage inversely provide new aisles for moisture, oxygen and chloride throughout the loosen corroding rebar-concrete interface, resulting in the secondary acceleration of corrosion process.

3.2 Time-frequency and entropy characteristics of AE signals

Early research on the AE monitoring mainly relied on the evaluation of traditional AE parameters, such as AEN and event rate (ER), as well as rise angle (RA) and average frequency (AF). Perceived apparent shift in measured parameters promoted to effectively recognize the corresponding damage stages. In addition to the variations of fundamental AE parameters, the time-frequency characteristics of the signal itself are also worthy of attention, which contain a lot of information related to the structural damage status.

Four typical AE waveforms are selected from the four artificially divided corrosion stages based on AEN mentioned above, as shown in Fig. 5. These waveforms are analyzed for revealing more details of the damage process. These four AE waveforms seem similar in the time domain with maximum magnitude around 500 mV and duration of 2 ms. The corresponding power spectral density (PSD) and normalized

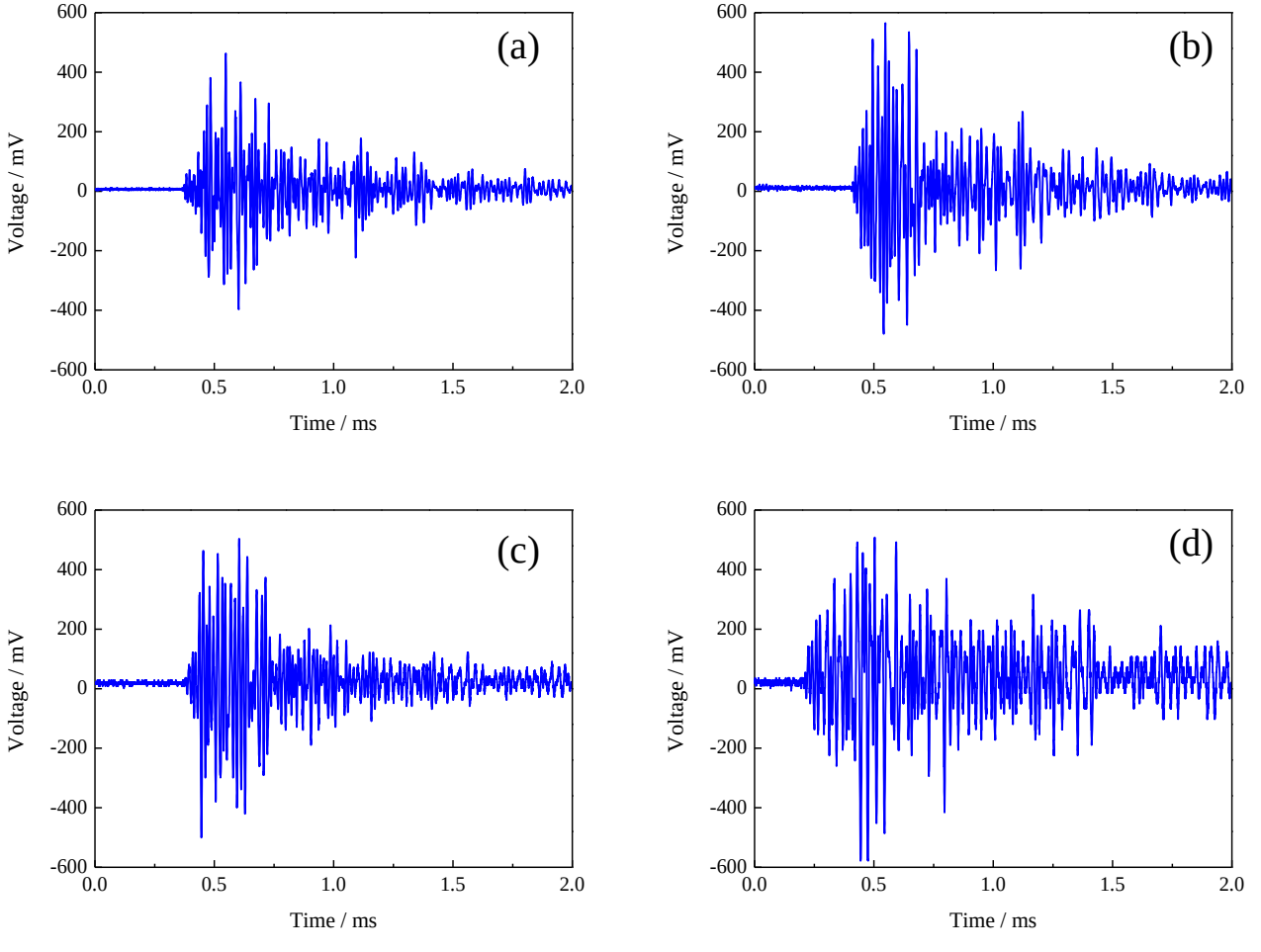

Fig. 5 Typical AE waveforms from the reinforced concrete beam. (a) Stage I, (b) Stage II, (c) Stage III and (d) Stage IV.

wavelet power contour maps of the four AE waveforms are shown in Figs. 6 and 7, respectively. In the spectral domain, the most obvious phenomenon was that the frequency band width becomes narrower continuously. At the first stage, there exist several apparent resonance peaks in the range of 150 kHz to 300 kHz. Based on the authors' previous research, the high-frequency components above 150 kHz are primarily attributed to the stress waves from corrosion and cracking of the metal oxide/hydroxide on the surface of steel reinforcement.[58] However, as the corrosion products accumulate on its surface, the corroding rebar-concrete interface gets loosened and simultaneously the surface stiffness reduces continuously due to the continuous oxidation of the iron atoms and ferrous ions, resulting in the attenuation and dissipation of high-frequency components above 150 kHz.

The normalized wavelet power contour map describes the energy distribution of AE signal in the time-frequency domain. The color bar in the normalized contour map is a linear scale, with dark red representing 100% and deep blue representing 5%. In the contour map of Fig. 7, the high-frequency components are almost imperceptible, and the main energy concentrates in the vicinity of 50 kHz. According to the classification method by Japan Construction Material Standards (JCMS) for active cracks in concrete, the low-frequency components at around 50 kHz are attributed to the tensile cracks of concrete materials.[59] In addition, it can be clearly seen that the center frequency gradually shifts from above 50 kHz to beneath 50 kHz. This phenomenon indicates that the mechanism of concrete deterioration is transforming from corrosion-induced micro cracking to load-induced localized cracking. The center frequency of acoustic emission is proportional to the dense microstructure of the concrete materials. At the early stage of corrosion process, the rust fills in the initial pores and defects and condenses the rebar-concrete interface. However, with the accumulation of corrosion products, once the over-expansion stress exceeds the tensile limit of the surrounding concrete, corrosion-induced micro-cracks initiate and propagate. The dense concrete microstructures correspond to the relatively high frequency characteristics (>50 kHz) of AE signal. Several corrosive wet-dry cycles afterwards, the rust pit appears and the effective cross-section area of reinforcement decreases, leading to the local stress concentration. Under the constant loading condition, the localized macro cracks grow and propagate. At this time, the relatively loosen concrete microstructures generate the low frequency features (<50 kHz) of AE waveform.

Equations (6~9) describes the calculation method of

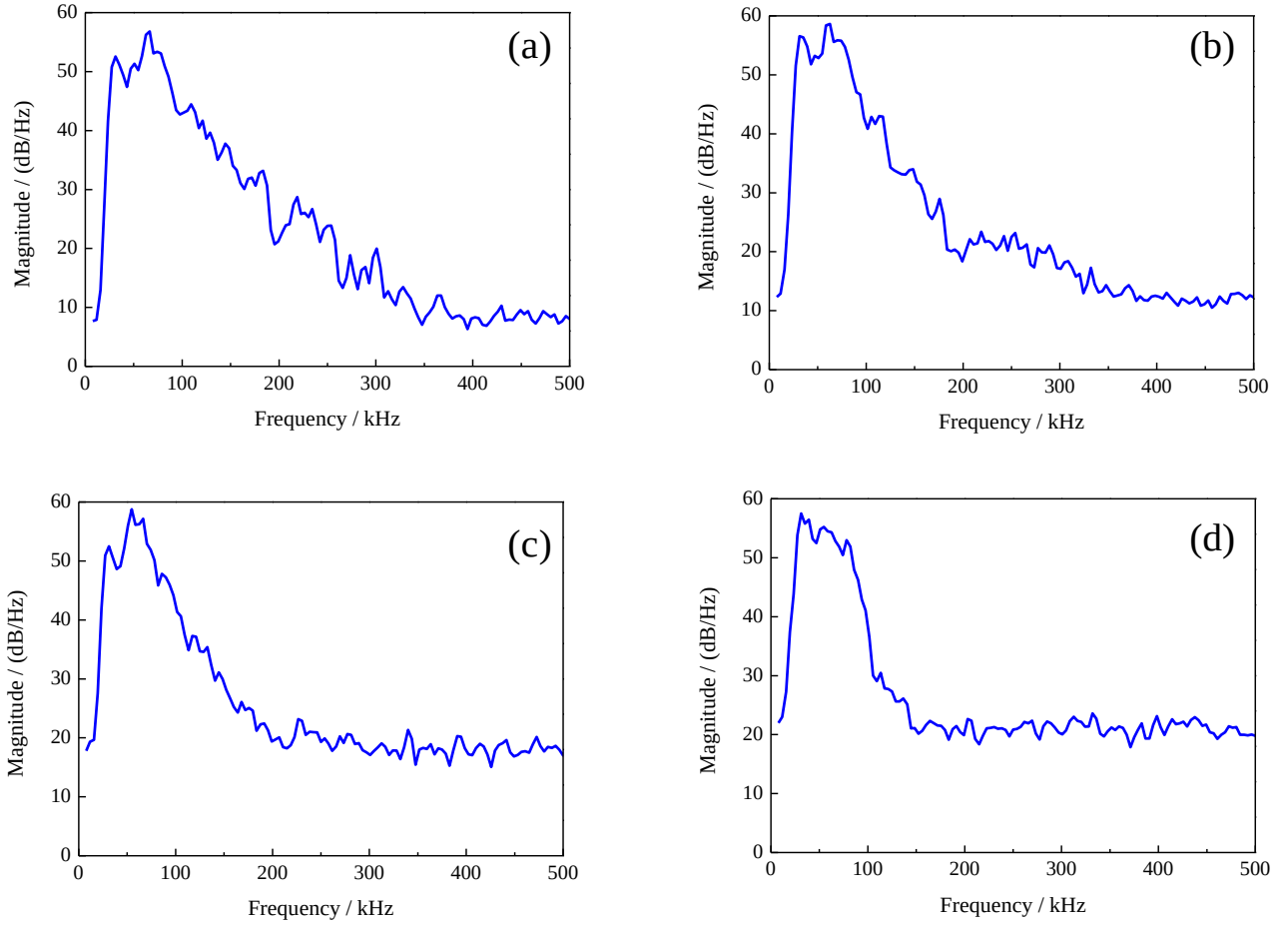

Fig. 6 PSD curves corresponding to the AE waveforms from the reinforced concrete beam. (a) Stage I, (b) Stage II, (c) Stage III and (d) Stage IV.

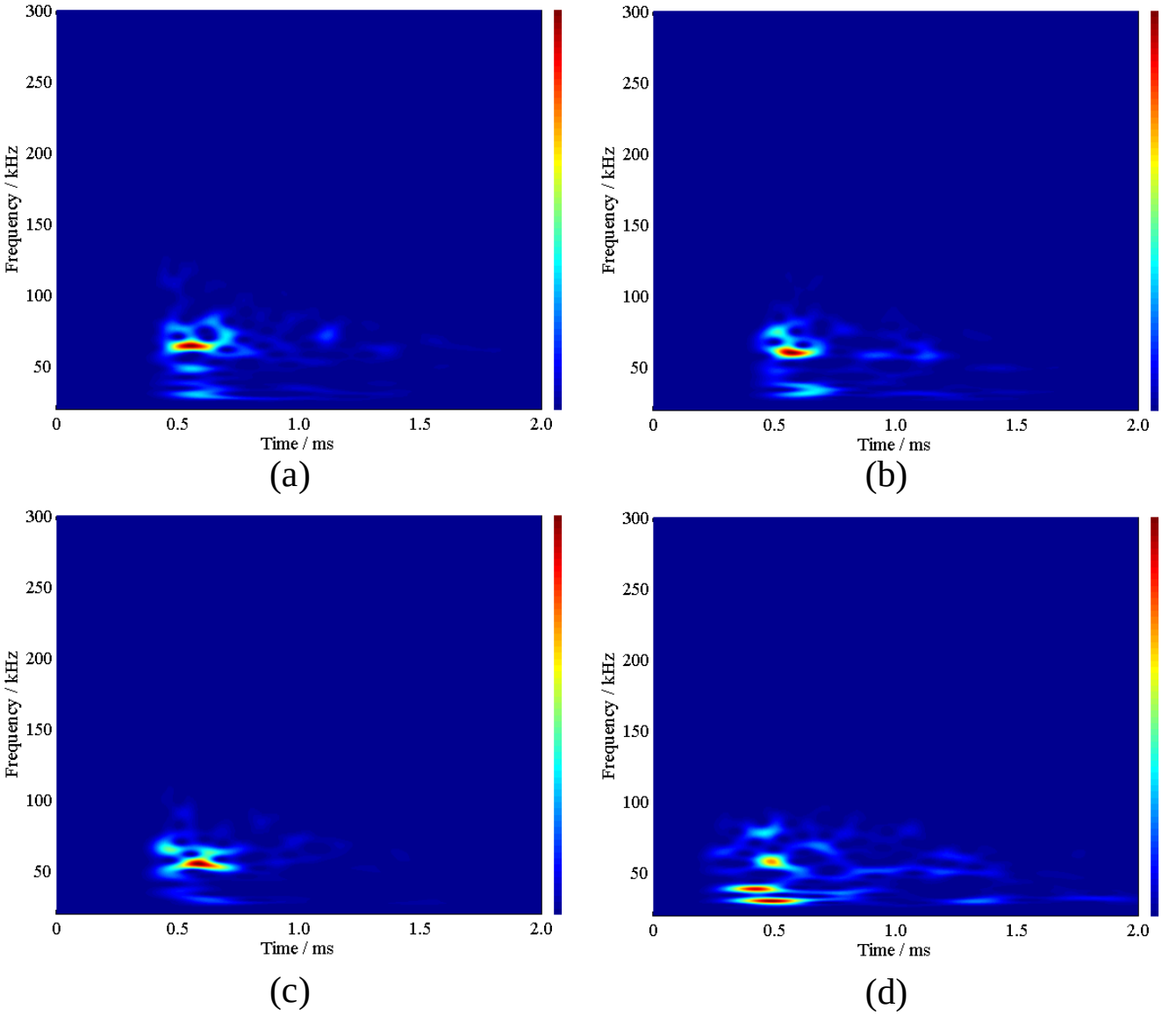

Fig. 7 Normalized wavelet power contour maps corresponding to the AE waveforms from the reinforced concrete beam. (a) Stage I, (b) Stage II, (c) Stage III and (d) Stage IV.

frequency-entropy using wavelet power. The frequency-entropy depends on how the wavelet power distributes with time variation in a certain frequency band. Based on the aforementioned formulas, if the wavelet power is perfectly uniformly distributed in time series within a certain frequency, it obtains the maximum value $Entropy = \log_2 N$ (N is the number in time series, equaling to 1000 in this study). However, if the power is highly centralized in one wavelet, it gets the minimum value $Entropy = 0$. Therefore, the wavelet entropy is normally within the range of 0 to $\log_2 N$. In other words, the higher entropy corresponds to relatively uniform distribution of wavelet power in time series within a certain frequency, while the lower entropy stands for the relatively concentrated distribution of wavelet power in time series within a certain frequency.

Fig. 8 shows the frequency-entropy curves corresponding to the wavelet power contour maps of Fig. 7. Although it is difficult to identify the energy variation of the wavelet power in the high frequency range of 150 kHz to 300 kHz in the contour image of Fig. 7, the change in the wavelet power distribution of the high-frequency components is well reflected in the frequency-entropy curve of Fig. 8. The mechanical wave attenuates with frequency during propagation, and the attenuation of high-frequency components is much more serious. Therefore, the energy of the high-frequency components is much smaller than that of the low-frequency components in the PSD curves. Compared with Fig. 6, the frequency-entropy curves in Fig. 8 clearly exhibit the relative power distribution of AE signal in the entire frequency region. As the concrete deterioration becomes more and more severe due to the coupling effects of steel corrosion and external bending moment, three distinguished phenomena can be summarized according to Fig. 8: (1) the frequency coordinate of the minimum entropy marked in red circle shifts to lower frequency band; (2) the magnitude of the minimum entropy gets larger but less apparent; (3) the

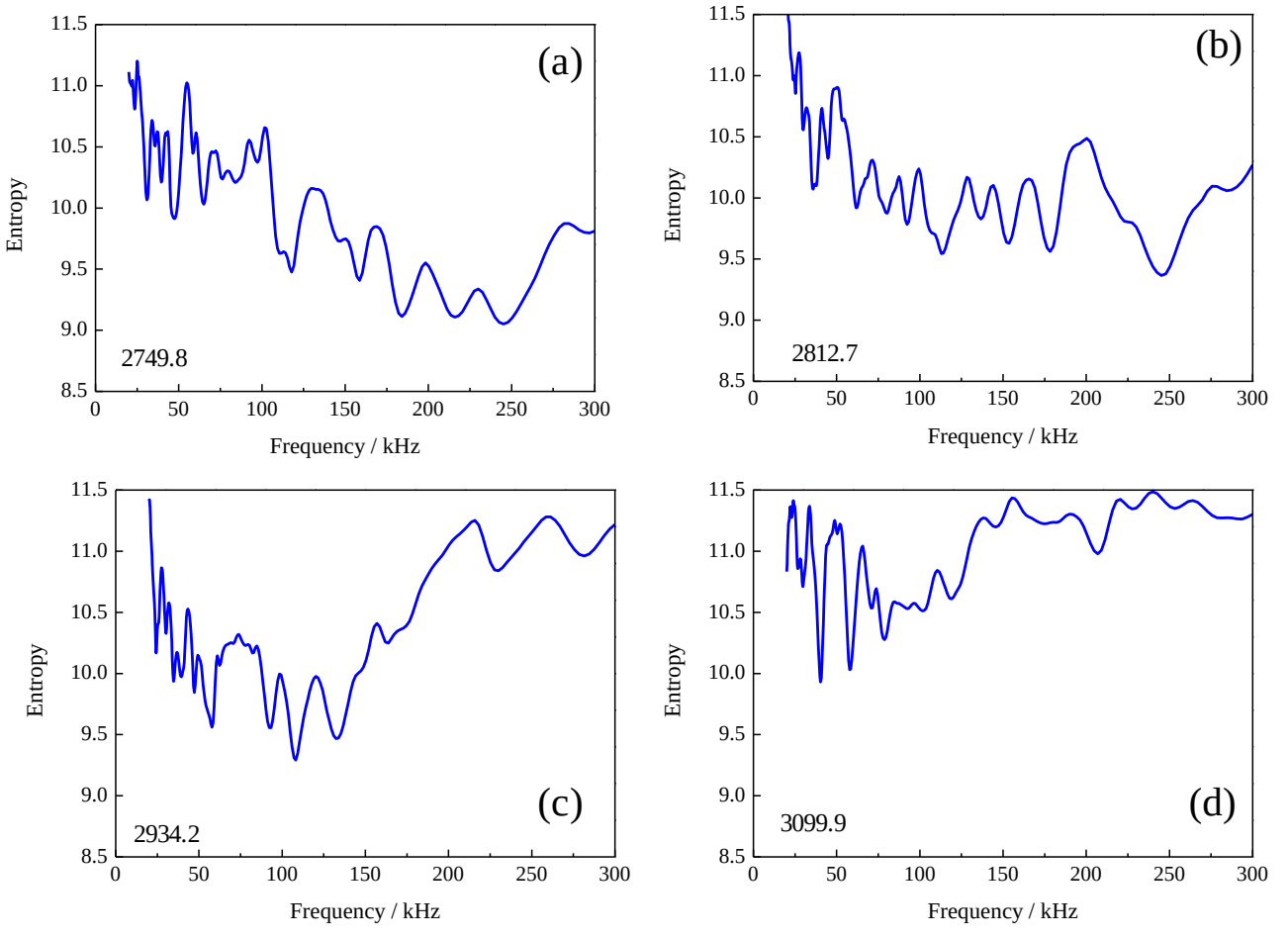

Fig. 8 Frequency-entropy curves of wavelet power corresponding to the contour maps of Fig. 7. (a) Stage I, (b) Stage II, (c) Stage III and (d) Stage IV.

increment of the overall entropy integration $\int Entropy(f) \cdot df$ is considerably evident, from 2749.8 to 3099.9. The increase of average entropy integration of AE signals following increasing number of wet-dry cycles is shown in Fig. 9. It can be seen that the overall trend is well consistent with Fig. 3.

The reinforced concrete structures are composed of steel reinforcement and concrete materials. Due to the distinction of material properties, steel and concrete have different AE characteristics. At the early stage of corrosion process, the concentrated distribution of wavelet power in high-frequency components is dominated by corrosion and cracking of the metal oxide/hydroxide on the surface of steel reinforcement, resulting in the minimum entropy in the high frequency region. Inversely, in the late period, the AE signal is governed by concrete cracking, which is in low frequency range with long duration. The variation of corresponding wavelet power is not quite violent, leading to higher minimum entropy in the low frequency region. The change of frequency-entropy curve corresponds to the revolution of damage degree of reinforced concrete structures subjected to the coupling effects of corrosive solution and external load, from corrosion-induced micro cracking to load-induced localized macro crack propagation. Therefore, wavelet power-based Shannon entropy is an effective approach to analyzing AE signals of reinforced concrete structures induced by steel corrosion and concrete cracking.

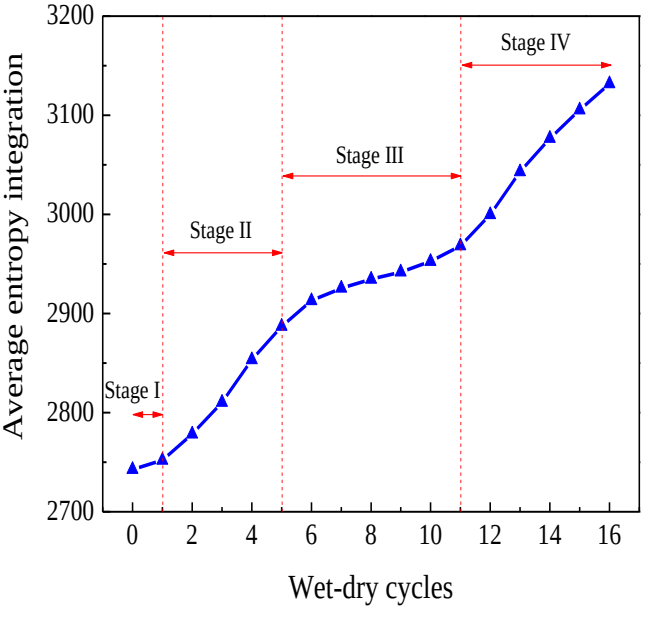

Fig. 9 Average entropy integration of AE signals during wet-dry cycles.

4. Conclusions

In this study, AE technique is employed to measure the corrosion and deterioration status of a loaded reinforced concrete beam subjected to wet-dry cycles of 3% NaCl solution. The following conclusions can be drawn:

(1) Based on the AEN curve over the corrosive wet-dry cycles of NaCl solution, the degradation process of the reinforced concrete beam can be divided into four stages: Stage I is chloride ions accumulation; Stage II is corrosion initiation and micro-cracks propagation; Stage III is corrosion rate reduction; and Stage IV is reinforcement performance degradation and localized macro-crack growth.

(2) The time-frequency characteristics of AE signals reflect the degradation mechanism of reinforced concrete subjected to the coupling effects of chloride-induced corrosion and external load, which is represented by a transforming from corrosion-induced micro cracking to load-induced localized cracking.

(3) Wavelet power-based Shannon entropy is an effective approach to analyzing AE signals of reinforced concrete structures induced by steel corrosion and concrete cracking. The frequency-entropy curve clearly exhibits the relative power distribution of AE signal in a certain frequency region. With the accumulation of steel corrosion and concrete deterioration, the increment of the overall entropy integration is considerably evident.

Acknowledgements

Financial support from the National Natural Science Foundation of China under the grants of 52078332, U2006223 and 51925805, from the Natural Science Foundation of Hebei Province under the grant of E2020402079, and from the Guangdong Provincial Key Laboratory of Durability for Marine Civil Engineering (SZU) under the grant of 2020B1212060074 is gratefully acknowledged.

Conflict of Interest

There is no conflict of interest.

Supporting Information

Not applicable.

References

[1] H. P. Zhu, H. Luo, D. M. Ai, and C. Wang, *Measurement,* 2016, **88**, 353-359, doi: 10.1016/j.measurement.2016.01.041.

[2] M. J. McCarthy, P. A. J. Tittle, and R. K. Dhir, *Cem. Concr. Compos.,* 2019, **102**, 71-83, doi: 10.1016/j.cemconcomp.2019.03.003.

[3] B. A. Salami, S. M. Rahman, T. A. Oyehan, M. Maslehuddin, and S. U. Al Dulaijan, *Measurement,* 2020, **165**, 108141, doi: 10.1016/j.measurement.2020.108141.

[4] G. F. Qiao, Y. Hong, and J. P. Ou, *Measurement,* 2015, **67**, 78-83, doi: 10.1016/j.measurement.2014.12.018.

[5] G. F. Qiao, Y. Hong, J. P. Ou, and X. C. Guan, *Measurement,* 2015, **67**, 84-91, doi: 10.1016/j.measurement.2014.12.048.

[6] A. Mohammadian, R. Rashetnia, G. Lucier, R. Seracino, and M. Pour-Ghaz, *Cem. Concr. Compos.,* 2019, **103**, 263-278, doi: 10.1016/j.cemconcomp.2019.04.027.

[7] B. J. Zhan, D. X. Xuan, W. L. Zeng, and C. S. Poon, *Cem. Concr. Compos.,* 2019, **104**, 103360, doi: 10.1016/j.cemconcomp.2019.103360.

[8] Z. K. Wang, J. Yu, G. Y. Li, M. Zhang, and C. K. Y. Leung, *Cem. Concr. Compos.,* 2019, **100**, 120-129, doi: 10.1016/j.cemconcomp.2019.02.013.

[9] X. F. Zhao, Y. J. Cui, H. M. Wei, X. L. Kong, P. L. Zhang, and C. S. Sun, *Smart Mater. Struct.,* 2013, **22**, 065014, doi: 10.1088/0964-1726/22/6/065014.

[10] H. F. Pei, Z. J. Li, J. R. Zhang, and Q. Wang, *Constr. Build. Mater.*, 2015, **93**, 989-994, doi: 10.1016/j.conbuildmat.2015.05.057.

[11] H. Al-Mattarneh, *Corros. Sci.*, 2016, **105**, 133-140, doi: 10.1016/j.corsci.2016.01.010.

[12] J. R. Zhang, C. Liu, M. Sun, and Z. J. Li, *Constr. Build. Mater.*, 2017, **135**, 68-75, doi: 10.1016/j.conbuildmat.2016.12.157.

[13] L. Fan, Y. Bao, W. N. Meng, and G. D. Chen, *Compos. B. Eng.*, 2019, 165, 679-689, doi: 10.1016/j.compositesb.2019.02.051.

[14] S. H. Jiang, H. Wang, and A. Z. Liu, *Measurement,* 2020, **164**, 16, 107994, doi: 10.1016/j.measurement.2020.107994.

[15] A. Meserkhani, S. M. Jafari, and A. Rahi, *Measurement,* 2021, **168**, 108198, doi: 10.1016/j.measurement.2020.108198.

[16] M. Ohtsu, K. Mori, and Y. Kawasaki, *Strain,* 2011, **47**, 179-186, doi: 10.1111/j.1475-1305.2010.00754.x.

[17] Y. Kawasaki, T. Wakuda, T. Kobarai, and M. Ohtsu, *Constr. Build. Mater.*, 2013, **48**, 1240-1247, doi: 10.1016/j.conbuildmat.2013.02.020.

[18] M. Karcili, N. Alver, and M. Ohtsu, *Mater. Struct.,* 2016, **49**, 2171-2178, doi: 10.1617/s11527-015-0641-3.

[19] V. Kietov, M. Mandel, and L. Kruger, *Adv. Eng. Mater.*, 2019, **21**, 1800682, doi: 10.1002/adem.201800682.

[20] R. Goldaran and A. Turer, *Measurement,* 2020, **160**, 8, 107855, doi: 10.1016/j.measurement.2020.107855.

[21] M. Ohtsu and Y. Tomoda, *ACI Mater. J.,* 2008, **105**, 194-199.

[22] Y. Y. Lu, Z. J. Li, and L. Qin, *ACI Mater. J.,* 2011, **108**, 178-186.

[23] M. Ohtsu, *Constr. Build. Mater.*, 2016, **122**, 845-854, doi: 10.1016/j.conbuildmat.2015.12.137.

[24] L. Djeddi, R. Khelif, S. Benmedakhene, and J. Favergeon, *Int. J. Electrochem. Sci.,* 2013, **8**, 8356-8370.

[25] E. Pomponi, A. Vinogradov, and A. Danyuk, *Signal Process.,* 2015, **115**, 110-119, doi: 10.1016/j.sigpro.2015.03.016.

[26] B. Dykas and J. Harris, *Mech. Syst. Signal Process.,* 2017, **93**, 397-414, doi: 10.1016/j.ymssp.2017.01.049.

[27] S. Gholizadeh, Z. Leman, and B. Baharudin, *Struct. Eng. Mech.,* 2015, **54**, 1075-1095, doi: 10.12989/sem.2015.54.6.1075.

[28] F. Hemmati, W. Orfali, and M. S. Gadala, *Appl. Acoust.,* 2016, **104**, 101-118, doi: 10.1016/j.apacoust.2015.11.003.

[29] L. Yang, T. T. Yang, Y. C. Zhou, Y. G. Wei, R. T. Wu, and N. G. Wang, *Surf. Coat. Technol.,* 2016, **304**, 272-282, doi:

10.1016/j.surfcoat.2016.06.080.
[30] T. M. Cover and J. A. Thomas, *Elements of Information Theory*, New York: Wiley, 2006.
[31] S. Ekici, S. Yildirim, and M. Poyraz, *Expert Syst. Appl.,* 2008, **34**, 2937-2944, doi: 10.1016/j.eswa.2007.05.011.
[32] A. K. Das and C. K. Y. Leung, *Cem. Concr. Compos.,* 2019, **104**, 103409, doi: 10.1016/j.cemconcomp.2019.103409.
[33] J. R. Zhang, Y. Y. Lu, Z. Y. Lu, C. Liu, G. X. Sun, and Z. J. Li, *Smart Mater. Struct.,* 2015, **24**, 025023, doi: 10.1088/0964-1726/24/2/025023.
[34] Y. Y. Lu, H. Y. Ma, and Z. J. Li, *J. Intell. Mater. Syst. Struct.* 2015, **26**, 280-291, doi: 10.1177/1045389x14525488.
[35] J. R. Zhang, T. Y. Fan, H. Y. Ma, and Z. J. Li, *Constr. Build. Mater.,* 2015, **88**, 118-125, doi: 10.1016/j.conbuildmat.2015.04.010.
[36] M. Z. Yuan, J. R. Zhang, L. Z. Yang, E. Q. Fang, Z. J. Li, and H. Ren, *Mater. Res. Innov.,* 2015, **19**, S134-S138, doi: 10.1179/1432891715z.0000000001389.
[37] D. J. Yoon, W. J. Weiss, and S. P. Shah, *J. Eng. Mech.,* 2000, **126**, 273-283, doi: 10.1061/(asce)0733-9399(2000)126:3(273).
[38] Y. Y. Lu, Z. J. Li, and L. Qin, *Comput. Concr.,* 2011, **8**, 563-581 doi: 10.12989/cac.2011.8.5.563.
[39] I. Daubechies, "Ten Lectures on Wavelets," ed: SIAM, Philadelphia, 1992.
[40] W. J. Yan and W. X. Ren, *J. Struct. Eng.,* 2013, **139**, 1444-1456, doi: 10.1061/(asce)st.1943-541x.0000711.
[41] "Matlab function reference. Matlab Ver. R2007a," ed: Mathwork Inc., 2007.
[42] R. Piotrkowski, E. Castro, and A. Gallego, *Mech. Syst. Signal Process.* 2009, **23**, 432-445, doi: 10.1016/j.ymssp.2008.05.006.
[43] X. Zhang, N. Z. Feng, Y. Wang, and Y. Shen, *J. Sound Vib.,* 2015, **339**, 419-432, doi: 10.1016/j.jsv.2014.11.021.
[44] J. K. Chen, Y. H. Dou, Y. Li, and J. Li, *Entropy,* 2016, **18**, 437, doi: 10.3390/e18120437.
[45] Z. J. Li, *J. Adv. Concr. Technol.*, Hoboken, New Jersey: John Wiley & Sons, Inc., 2011, 624.
[46] Y. X. Zhao, J. F. Dong, H. J. Ding, and W. L. Jin, *Corros. Sci.,* 2015, **98**, 310-317, doi: 10.1016/j.corsci.2015.05.028.
[47] L. Calabrese, M. Galeano, E. Proverbio, D. Di Pietro, F. Cappuccini, and A. Donato, *Corros. Sci.,* 2016, **111**, 151-161, doi: 10.1016/j.corsci.2016.05.010.
[48] D. G. Aggelis, D. V. Soulioti, N. M. Barkoula, A. S. Paipetis, and T. E. Matikas, *Cem. Concr. Compos.,* 2012, **34**, 62-67, doi: 10.1016/j.cemconcomp.2011.07.003.
[49] A. Sharma, S. Sharma, and A. Mukherjee, *Cem. Concr. Compos,* 2018, **90**, 89-99, doi: 10.1016/j.cemconcomp.2018.03.014.
[50] E. Tsangouri and D. G. Aggelis, *Constr. Build. Mater.,* 2019, **224**, 198-205, doi: 10.1016/j.conbuildmat.2019.07.042.
[51] R. E. Melchers and C. Q. Li, *ACI Mater. J.,* 2006, **103**, 1, 25-32.
[52] Y. M. Chen and M. E. Orazem, *Corros. Sci.,* 2016, **104**, 26-35, doi: 10.1016/j.corsci.2015.11.027.
[53] Z. Y. Ai, J. Jiang, W. Sun, X. Jiang, B. Yu, K. Wang, Z. Zhang, D. Song, J. Zhang, *Cem. Concr. Compos.,* 2018, **92**, 178-187, doi: 10.1016/j.cemconcomp.2018.06.005.
[54] J. R. Zhang, M. Sun, D. S. Hou, and Z. J. Li, *Constr. Build. Mater.*, 2017, **139**, 365-373, doi: 10.1016/j.conbuildmat.2017.02.064.
[55] J. Williamson and O. B. Isgor, *Corros. Sci.,* 2016, **106**, 82-95, doi: 10.1016/j.corsci.2016.01.027.
[56] R. E. Melchers, *J. Infrastruct. Syst.,* 2006, **12**, 154-162, doi: 10.1061/(asce)1076-0342(2006)12:3(154).
[57] B. Q. Dong, G. Shi, P. Dong, W. Ding, X. Teng, S. Qin, Y. Liu, F. Xing, S. Hong, *Cem. Concr. Compos.,* 2018, **92**, 102-109, doi: 10.1016/j.cemconcomp.2018.06.003.
[58] J. R. Zhang, H. Y. Ma, H. F. Pei, and Z. J. Li, *Mag. Concr. Res.,* 2017, **69**, 35-45, doi: 10.1680/jmacr.15.00496.
[59] JCMS-III B5706: Monitoring method for active cracks in concrete by acoustic emission, Japan, 2003.

Author information

Hongyan Ma *is an Associate Professor of civil/materials engineering at Missouri University of Science and Technology. His current research interests include future cements, durability of concrete, functional materials, smart materials and systems, multi-scale simulation, thermal energy storage, and large-scale CO_2 utilization and storage.*